World Journal of Advanced Research and Reviews
eISSN: 2581-9615 CODEN (USA): WJARAI
Cross Ref DOI: 10.30574/wjarr
Journal homepage: https://wjarr.com/

(RESEARCH ARTICLE)

Check for updates

Investigation of the mechanical properties and propagation of cracks in prosthetic teeth composed of porcelain and dental ceramics using cohesive meshing under quasi-static loading conditions

Mahdi Ahmadi * and Alireza Maghroor Porkar Abatari

Department of Mechanical Engineering, University of Gilan, Rasht, Gilan, Iran.

World Journal of Advanced Research and Reviews, 2024, 21(03), 1335–1346

Publication history: Received on 05 February 2024; revised on 13 March 2024; accepted on 15 March 2024

Article DOI: https://doi.org/10.30574/wjarr.2024.21.3.0848

Abstract

With the significant progress in dental science and the reliance of dental researchers on understanding the mechanical properties and behaviors of teeth and materials used for tooth replacement, there is an increasing demand for study and research in this sector. Composite samples, dental porcelains, and materials used in 3D printers have gained significance as substitutes for human teeth. Therefore, it is crucial to conduct research and analyze these materials' physical and mechanical characteristics compared to human teeth. Tooth damage and fracture may arise from various causes, such as falls, sports-related incidents, or traffic accidents. Tooth fractures may vary in severity, ranging from mild fractures that include chipping of the tooth's surface layers, known as enamel and dentin, to more serious ones, such as diagonal, vertical, or horizontal fractures extending into the root of the tooth.

Keywords: Dental Science; Mechanical Properties; Tooth Replacement; Composite Sample; Tooth Fractures; Material Analysis

1. Introduction

According to the quasi-static pressure experimental test done by Hian Lee et al. [1], this part examines the simulation of a three-dimensional artificial plastic tooth sample. This simulation investigates the crack propagation process in a tooth with a significant vertical fracture [2-5]. Additionally, it explores the application of cohesive components to determine the maximum force needed to commence damage and eliminate these cohesive elements [6-9]. This research focuses on determining the time of damage onset and how crack growth occurs by establishing a set of parameters. Laboratory methods are employed to determine the properties of various materials [10-15]. These properties are then used to model the direction of the tooth sample using cohesive meshing techniques [16, 17]. Below is a concise overview of the methodology used in conducting these tests. Various mechanical testing techniques are used to quantify the mechanical characteristics of teeth [18-23]. These methodologies result in distinct strategies for analyzing data. Further information is essential to comprehend the mechanical characteristics and tooth replacement materials [24].

- Assessment of the mechanical qualities and subsequent comparison with other materials [25, 26]
- Assessing and contrasting the appropriateness of alternative materials, such as alloys, ceramics, and metals, for dental applications [27, 28]
- Determining the key factors that alter the characteristics of tooth and replacement materials [29-32]

Hence, the techniques used for measuring must be comparable. The tooth has specific mechanical characteristics associated with its role in concentrating internal stresses on the tooth surface [33-37]. Numerous research has been undertaken to examine the mechanical characteristics of human teeth [38, 39]. Nevertheless, the processes by which teeth get deformed are still not well understood. Comprehending the connections among composition, structure, and

* Corresponding author: Mehdi Ahmadi

mechanical characteristics at the nanoscale is crucial for advancing novel biological materials [40]. The mechanical characteristics of human teeth, particularly the structure of various components, provide a complex material that is difficult to explain and compare. Their structure is intricate, consisting of several layers and components. At a large scale, the tooth looks like a uniform solid substance. At a microscopic level, the tooth comprises many components, including dentin, enamel, and others. These components consist of bundles of rod-shaped structures embedded in a matrix of water and protein. The mechanical characteristics of this material are similar to those of composite materials, such as ceramics or titanium nitride. Researchers [41] showed that tooth features undergo alterations based on the orientation of prisms. The tables below summarize the average values for teeth and other materials.

Table 1 Modulus of elasticity for teeth and engineering materials

	Scale	**Method**	**Sample**	**Occlusal plate [GPa]**	**Pivot plate [Gpa]**
Enamel section	Macroscopic	Pressure test	Molar teeth	84.2±6.2	78±4.8
	Microscopic	Modified Vickers indentation	Molar teeth	94±5	80±4
	Nano	Nanoindentation	Molar teeth	87.5±2.2	72.7±4.5
Engineering materials section	Microscopic	Modified Vickers indentation	ceramic	65±1.5 to 265±10	-
	Nano	Nanoindentation	porcelain	199.54±12.5	-

Table 2 Fracture toughness for teeth and engineering materials

	Scale	**Method**	**Sample**	**Occlusal plate [GPa]**	**Pivot plate [Gpa]**
Enamel section	Microscopic	Modified Vickers indentation	Molar teeth	0.77±0.05	0.52±0.06
Engineering materials section	Microscopic	Modified Vickers indentation	ceramic	1.2±0.14	-
			porcelain	7.4±0.62	

Table 3 Maximum value of tensile stress for teeth and engineering materials

	Scale	**Method**	**Sample**	**Occlusal plate [GPa]**	**Pivot plate [Gpa]**
Enamel section	Macroscopic	3 points Bending	Enamel section	49±17 to 68±16	-
	Microscopic	Micro-cantilever	Enamel section	750±240 to 1420±410	560±16 to 412±37
Engineering materials section	Microscopic	3 points Bending	ceramic	106±17	
			porcelain	840±140	

2. Failure through cohesive zone modeling

The fracture mechanics addressed so far have been grounded on the principles of continuum mechanics. This technique is a distinctive approach to failure analysis in fracture mechanics. It involves inducing a localized thickening at the crack tip and observing the fracture progression via an elimination process. The main objective of this method is to elucidate the underlying mechanism. Failure occurs when the fracture tip's stress concentration is exceptionally high or

concentrated in a single place. This region consists of two sticky surfaces wholly isolated from one other due to the tension of the adhesive area. The Separation is determined by an adhesive law that correlates the adhesive tension and the relative displacement of the surfaces.

Consequently, fracture propagation begins whenever the displacement is above a critical threshold. Attain the apex of the tangible fissure. The cohesive zone concept was first proposed by Dugdale in 1960 and Barnblatt in 1962 [42]. Scientists may acquire data on the cohesive elements, maximum tension, maximum Separation, and sample form via laboratory tests governed by many rules. Fourteen Generally, a cohesive law is a mathematical representation that defines the correlation between cohesive tension and separation displacement. This connection is often written in the form of equation (1).

$$\sigma = \sigma_c f(\frac{\delta}{\delta_c}) \tag{1}$$

Where σ_c denotes the maximum tensile stress exerted, and in the natural surroundings, it signifies the point at which fracture initiation occurs. f is a dimensionless separation function represented by the symbol δ_c characterizes the form of the tensile stress and separation diagram [43]. Figure 1 Different graphs of tensile stress and Separation for element Cohesion have been exhibited.

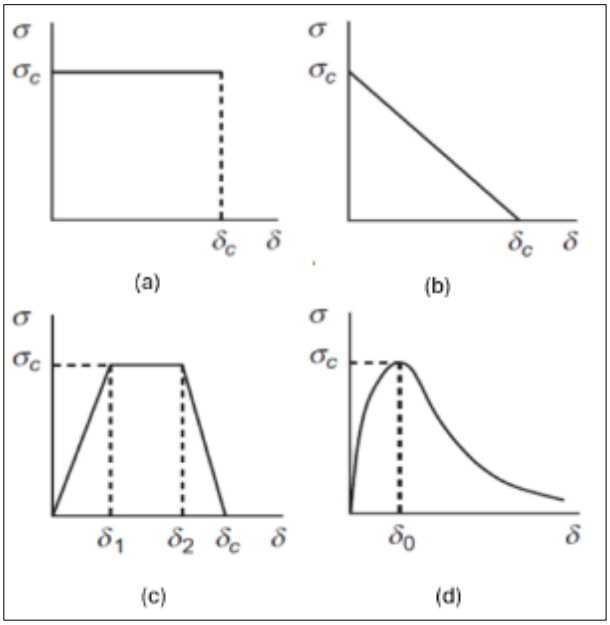

Figure 1 Tensile stress diagram - separation: (a): Dogdale model, (b): soft linear model, (c): trapezoidal model, and (d): exponential model

$$\sigma = \sigma_c \quad \text{Dogdale model (2)}$$

$$\sigma = \sigma_c(1 - \frac{\delta}{\delta_c}) \quad \text{Linear model (3)}$$

$$\sigma = \sigma_c \left(\frac{\delta}{\delta_c}\right) exp(1 - \frac{\delta}{\delta_c}) \quad \text{Exponential model (4)}$$

The trapezoidal model integrates the continuous linear model with the Dugdale model. The energy density of each model is determined by calculating the area under the curve. This may be done using primary geometric forms or by integrating the fracture energy curve. A primary constraint of cohesive zone modeling is relying on experimental data to determine most of the involved parameters. Initially implemented for nonlinear fracture modeling, this approach has since found extensive use in materials science for simulating adhesion, delamination, and even polymers.

2.1. Accurate modeling

As the introduction states, this study utilizes DCOM photos for modeling purposes. The DCOM standard, provided by the National Association of Electronic Equipment Manufacturers, facilitates the visualization and replication of medical images, including CT and MRI scans. A DCOM file has comprehensive patient information, including scan type, picture

dimensions, and image data: magnetic Resonance Imaging (MRI) and Computed Tomography (CT). Software like Erisis, Medkan, and Mimix can transform DCOM photos into a format that can be analyzed. For this study, we worked with Dr. Hossein Hosseini Zare's Maxillofacial Radiology Center in Mashhad to generate pictures in DCOM and STL formats. The following passage provides a concise overview of the procedure for using these pictures in Mimix software. Mimix is a program specialized in 3D image processing that handles all the typical scanner formats. One of the components of this program is Modcode, which facilitates the transformation of CT and MRI pictures into a compatible format for use in finite element software settings. The Mimax software displays the positioning of the CT pictures of Maryam Resalati, a 31-year-old patient. It is essential to ascertain their orientation to ensure proper picture rendering in the program. It is necessary to provide parameters while doing imaging. However, there are instances when the provided information is insufficient, and it becomes necessary to ascertain this information comprehensively, including all orientations, such as right, left, front, rear, higher, and lower.

Figure 2 How to place CT photos in Mimix software

2.1.1. Separation of the jaw and teeth

For this study, partitioning masks are used to isolate certain desirable regions in order to focus on a particular tooth. Various masks may be seen as spectacles of varying hues. The targeted regions are chosen by establishing the gray value range or the Hounsfield number. The bounds of these zones are defined by the Hansfield numbers that fall within the specified range. A mask encompasses all the pixels within this range. This method makes it possible to differentiate between soft and hard tissue. Figure (3) clearly illustrates the patient's jaw and teeth region.

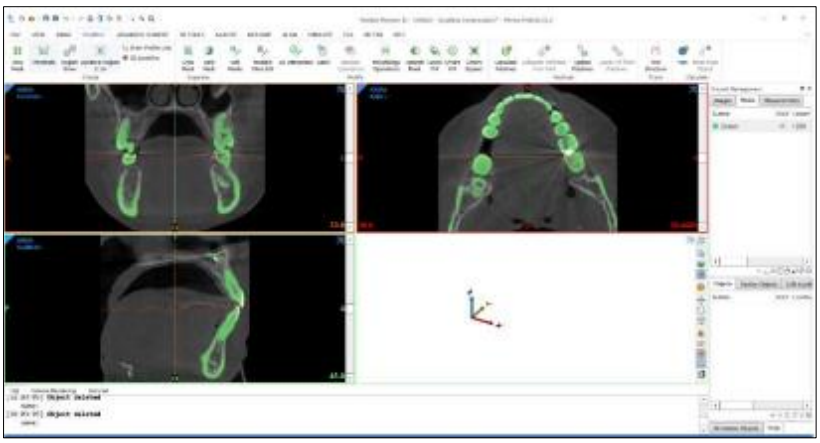

Figure 3 The section of the patient's jaw and teeth with the selection of a mask

Using the software modules, the second molar tooth, located in the lower jaw, was removed for engineering examination. Figure 4 displays the chosen tooth sample, as seen below.

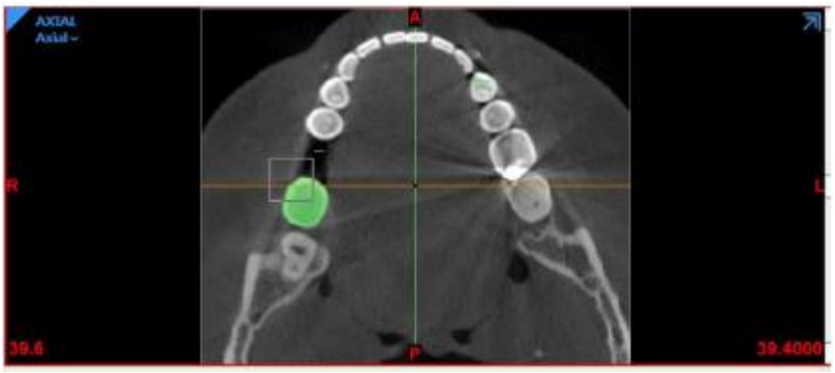

Figure 4 Bottom view of the selected second molar tooth

Once the sample for the 3D model has been chosen and prepared, it is introduced into a software environment known as Metric. Metric offers a range of functions, including surface smoothing, hole filling, and removing any unnecessary protrusions on the sample. Furthermore, the necessary modifications have been implemented to the sample, rendering it seamless and prepared for generating grids in the analysis program.

2.2. WJS Heading level 2

In this part, the modeling of the tooth sample has been conducted based on the experimental quasi-static pressure test performed by Hian Lee et al.[1]. The introductory portion of this simulation provides a comprehensive explanation of the crack propagation in a tooth with a significant vertical fracture. Cohesive elements compute the maximal force needed to commence damage and remove cohesive components.

2.2.1. Prototyping

The part module in Abaqus software generates the geometric representation of the requested component or components for analytical purposes. The offered 3D tooth component module separates it into three sections using the available capabilities and techniques. The crack expansion and damage occurred in the cohesive region of the tooth, namely in the left, right, and center parts. The chosen shape is designated as deformable, and the quasi-static pressure testing system, including a power lever and tooth holder, is used in this modeling according to the ASTM 7298 standard.

Figure 5 Sample of tooth brought for analysis

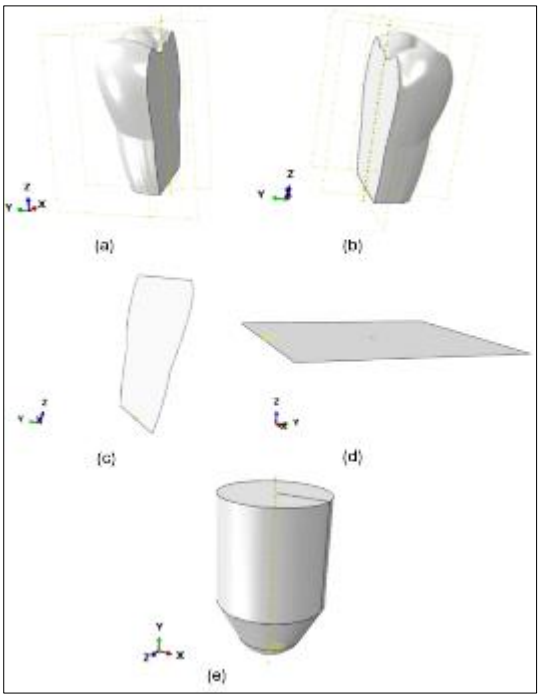

Figure 6 Tooth modeling in the part section: (a) the left side of the tooth, (b) the right side of the tooth, (c) placement of cohesive elements in the center of the tooth, (d) holder for teeth, (e) force lever for quasi-static pressure test

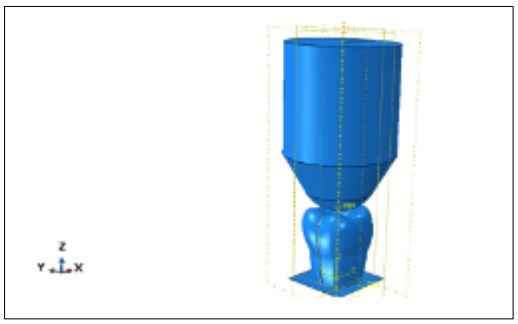

Figure 7 System designed for quasi-static pressure testing

2.2.2. Determining the properties of matter

This section provides the characteristics of four materials used in the dental examination and three materials associated with the standard examination for metals. The parameters included for this modeling are elastic modulus, Poisson's ratio, density, maximum tensile stress, yield stress, and stress intensity factor.

Table 4 Properties of materials used in tooth modeling

Material	$E[Mpa]$	v	$\rho[\frac{ton}{mm^3}]$	$\sigma_{uts}[Mpa]$	$k[\frac{kN}{mm}]$
Tooth	69000	0.3	2.5×10^9	30	3.2
porcelain	67000	0.3	2.3×10^9	130	2
ceramic	64000	0.3	2.2×10^9	62	1.4

2.2.3. Uploading

The tooth sample underwent a quasi-static pressure test, during which the roots were fully extracted, and the sample was stored at the initial region of the roots. The Instron general test equipment has a pressure lever that conforms to the standard and has been simulated.

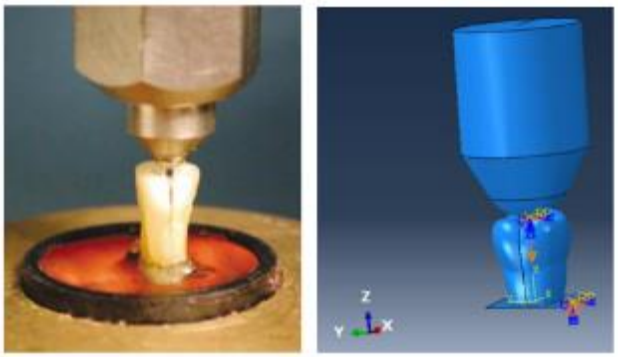

Figure 8 How to hold and load the tooth according to the test with the Instron machine

2.2.4. Networking

The grids included in the Abaqus software library are used for several categories of geometric models. This modeling focused on transferring the model from the interface to the analytical software. The model was represented as a collection of points and a grid called orphan mesh 2. This orphan mesh two was then converted into a complete model, also known as part 1, using specific command codes associated with the grid. Due to the model's intricate nature and several curves, the program could not choose an appropriate technique to generate grids using cubic or mostly cubic components for all sections of the model. This study focuses on enhancing the meshing capabilities of the model by effectively dividing the piece and using various tools in the meshing module, such as virtual topology. The program can now mesh the piece with cubic components by employing the suitable method. Sweep grids are essential for both the cohesive portion and the central area of the tooth. A three-dimensional grid, under strain and depending on the second degree, has been used in the separated parts of the left and right teeth.

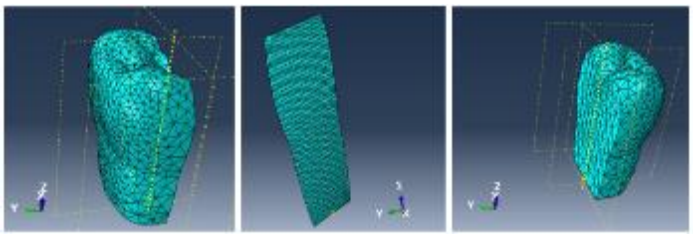

Figure 9 Networking of different parts of the sample

3. Results

The following analysis investigates the force diagram of three samples by considering the attributes of teeth, porcelain, and ceramics.

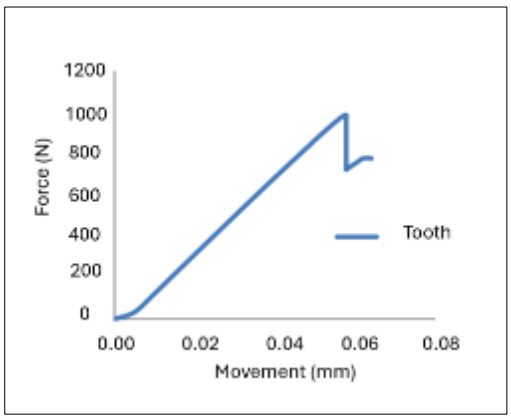

Figure 10 Diagram of force in terms of displacement for teeth

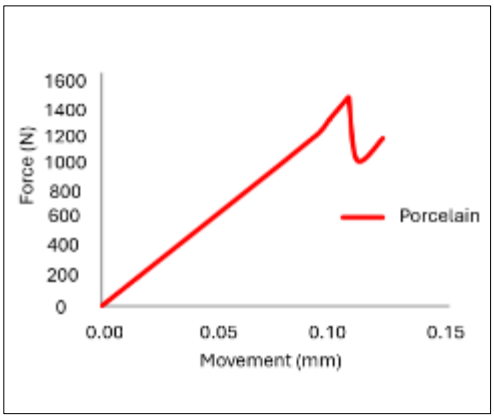

Figure 11 Force diagram in terms of displacement for porcelain

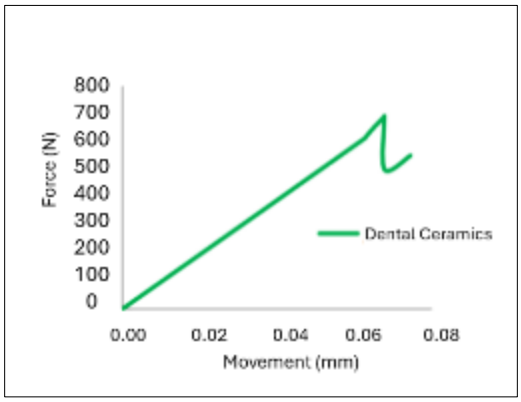

Figure 12 Force diagram according to displacement for dental ceramics

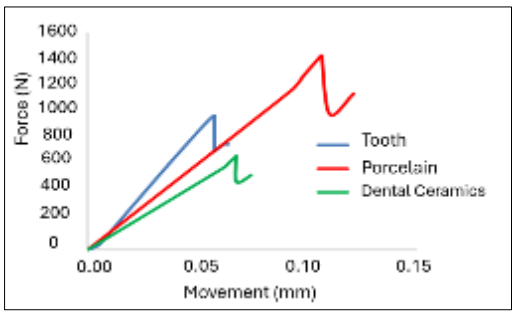

Figure 13 Comparative diagram of displacement force of three samples

Figures (10) to (13) demonstrate that the power and displacement required to initiate dental porcelain damage are more significant than in ceramics and natural human teeth. This makes dental porcelains a viable alternative for replacement. Consequently, artificial teeth and low-code porcelain are often used today. The shown figures illustrate the outlines of the maximum primary stress for the given samples.

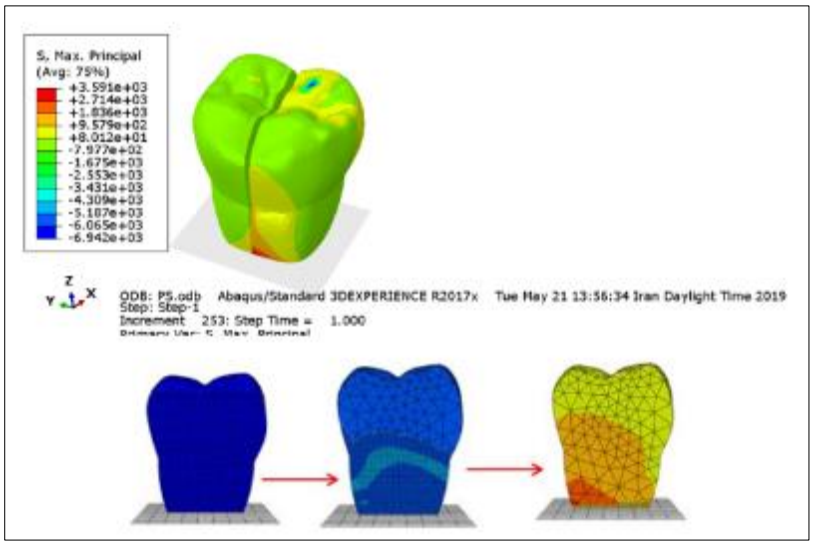

Figure 14 The contour of the maximum main stress and how to remove the cohesive elements of human teeth

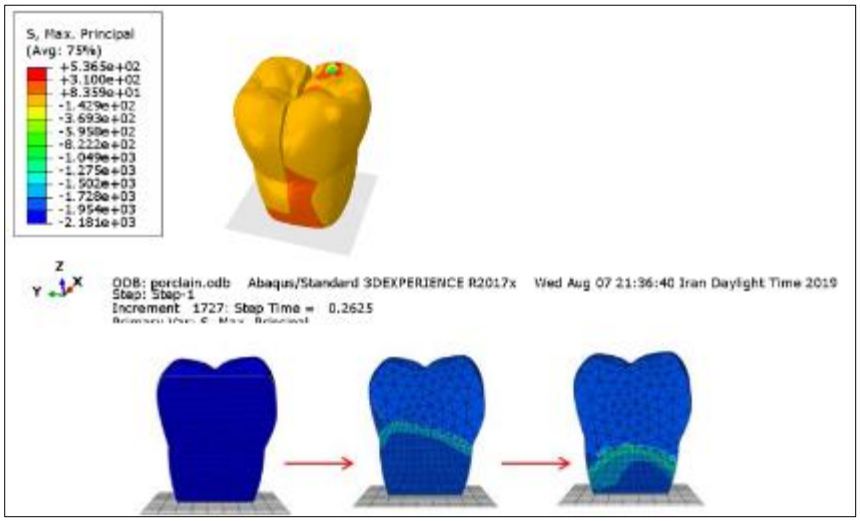

Figure 15 The contour of the maximum main stress and how to target the cohesive elements of dental porcelain

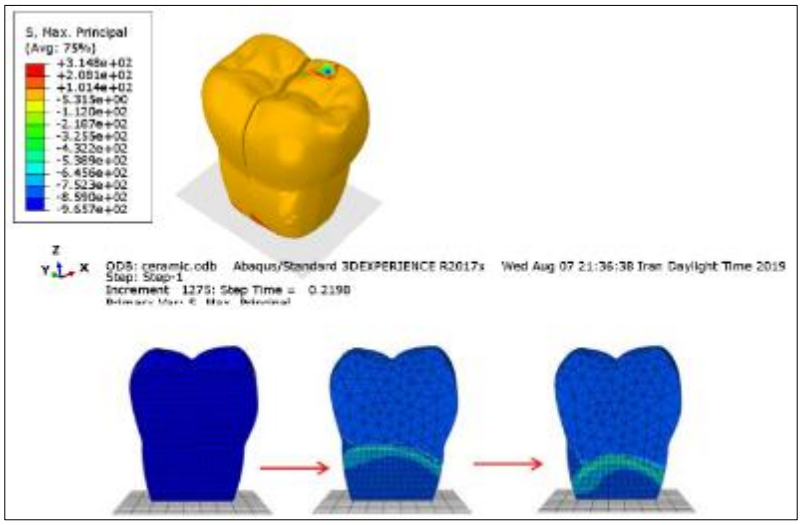

Figure 16 The contour of the maximum main stress and how to remove dental ceramic cohesive elements

Compliance with ethical standards

Disclosure of Conflicting Interests

The author(s) declared no conflicts of interest to disclosed.

References

[1] Li, H.; Li, J.; Zou, Z.; Fok, A. S.-L., Fracture simulation of restored teeth using a continuum damage mechanics failure model. Dental materials 2011, 27 (7), e125-e133.

[2] Alvandifar, N.; Saffar-Avval, M.; Amani, E.; Mehdizadeh, A.; Ebrahimipour, M.; Entezari, S.; Namazi, H.; Esfandiari-Mehni, M.; Ahmadibeni, G., Experimental study of partially metal foam wrapped tube bundles. International Journal of Thermal Sciences 2021, 162, 106798.

[3] Aminnia, N., CFD-XDEM coupling approach towards melt pool simulations of selective laser melting. 2023.

[4] Babazadeh Dizaj, R. DEVELOPMENT OF LSF-BASED DUAL-PHASE CATHODES FOR INTERMEDIATE TEMPERATURE SOLID OXIDE FUEL CELLS. Middle East Technical University, 2022.

[5] Bhuvela, P.; Taghavi, H.; Nasiri, A. In Design Methodology for a Medium Voltage Single Stage LLC Resonant Solar PV Inverter, 2023 12th International Conference on Renewable Energy Research and Applications (ICRERA), IEEE: 2023; pp 556-562.

[6] Aminnia, N.; Adhav, P.; Darlik, F.; Mashhood, M.; Saraei, S. H.; Besseron, X.; Peters, B., Three-dimensional CFD-DEM simulation of raceway transport phenomena in a blast furnace. Fuel 2023, 334, 126574.

[7] Aminnia, N.; Estupinan Donoso, A. A.; Peters, B., Developing a DEM-Coupled OpenFOAM solver for multiphysics simulation of additive manufacturing process. Scipedia. com 2022.

[8] Aminnia, N.; Estupinan Donoso, A. A.; Peters, B., CFD-DEM simulation of melt pool formation and evolution in powder bed fusion process. 2022.

[9] Chalaki, H. R.; Babaei, A.; Ataie, A.; Seyed-Vakili, S.-V. In The Effect of Impregnation of Ceramic Nano-particles on the Performance of LSCM/YSZ Anode Electrode of Solid Oxide Fuel Cell, 5th International Conference on Materials Engineering and Metallurgy, 2016.

[10] Dizaj, R. B.; Sabahi, N., Optimizing LSM-LSF composite cathodes for enhanced solid oxide fuel cell performance: Material engineering and electrochemical insights. 2023.

[11] Dizaj, R. B.; Sabahi, N., Laboratory preparation of LSM and LSF sputtering targets using PTFE rings for deposition of SOFC thin film electrodes. World Journal of Advanced Engineering Technology and Sciences 2023, 10 (2), 203-212.

[12] Khodabakshi, Z.; Nazari, B.; Taghavijeloudar, M. In Adding micronutrient of FeCl 2 and ZnCl 2 to culture medium in order to enhance high-value bioproduct extraction from microalgae, 13th international conference on new solutions in engineering, information science & technology of the century ahead, 2022.

[13] Rostaghi Chalaki, H.; Babaei, A.; Ataie, A.; Seyed-Vakili, S. V., LaFe 0.6 Co 0.4 O 3 promoted LSCM/YSZ anode for direct utilization of methanol in solid oxide fuel cells. Ionics 2020, 26, 1011-1018.

[14] Mahamud, R.; Mobli, M.; Farouk, T. I. In Modes of oscillation in a high pressure microplasma discharges, 2014 IEEE 41st International Conference on Plasma Sciences (ICOPS) held with 2014 IEEE International Conference on High-Power Particle Beams (BEAMS), IEEE: 2014; pp 1-6.

[15] mahmoodreza Hashemi, S.; Aminnia, N.; Derakhshan, S., Optimization Design of Pumps as Turbines (PATs) Arrays in a Water Distribution Network Aiming Energy Recovery.

[16] Mobli, M., Thermal analysis of high pressure micro plasma discharge. 2014.

[17] Mobli, M. Characterization Of Evaporation/Condensation During Pool Boiling And Flow Boiling. University of South Carolina, 2018.

[18] 18. Mobli, M.; Bayat, M.; Li, C., Estimating bubble interfacial heat transfer coefficient in pool boiling. Journal of Molecular Liquids 2022, 350, 118541.

[19] Mobli, M.; Farouk, T. In High pressure micro glow discharge: Detailed approach to gas temperature modeling, APS Annual Gaseous Electronics Meeting Abstracts, 2014; p KW2. 006.

[20] Mobli, M.; Li, C. In On the heat transfer characteristics of a single bubble growth and departure during pool boiling, International Conference on Nanochannels, Microchannels, and Minichannels, American Society of Mechanical Engineers: 2016; p V001T04A006.

[21] Aminnia, N.; Peters, B.; ESTUPINAN, A. A., Multi-Scale Modeling of Melt Pool Formation and Solidification in Powder Bed Fusion: A Fully Coupled Computational Fluid Dynamics-Extended Discrete Element Method Approach. Available at SSRN 4502227.

[22] Aminnia, N.; Shateri, M.; Gheibi, S.; Torabi, F., Modeling of Two-Phase flow in the Cathode Gas Diffusion Layer to Investigate Its Effects on a PEM Fuel Cell.

[23] Mobli, M.; Mahamud, R.; Farouk, T. In High pressure micro plasma discharge: Effect of conjugate heat transfer, 2013 19th IEEE Pulsed Power Conference (PPC), IEEE: 2013; pp 1-6.

[24] O'Brien, S.; Keown, A. J.; Constantino, P.; Xie, Z.; Bush, M. B., Revealing the structural and mechanical characteristics of ovine teeth. journal of the mechanical behavior of biomedical materials 2014, 30, 176-185.

[25] Nakhi, A.; Ganjali, M.; Shirinzadeh, H.; Sedaghat Ahangari Hossein Zadeh, A.; Mozafari, M., Laser Cladding of Fluorapatite Nanopowders on Ti6Al4V. Advanced Materials Letters 2020, 11 (1), 1-5.

[26] Nakhi, A.; Mostafa, S.; Karimi, A.; Mobli, M., Unveiling the Promoted LSTM/YSZ Composite Anode for Direct Utilization of Hydrocarbon Fuels. International Journal of Science and Engineering Applications 2023, 12 (12), 18 - 24.

[27] Namazi, H.; Perera, L. P. In Trustworthiness Evaluation Framework for Digital Ship Navigators in Bridge Simulator Environments, International Conference on Offshore Mechanics and Arctic Engineering, American Society of Mechanical Engineers: 2023; p V005T06A037.

[28] Namazi, H.; Taghavipour, A., Traffic flow and emissions improvement via vehicle-to-vehicle and vehicle-to-infrastructure communication for an intelligent intersection. Asian Journal of Control 2021, 23 (5), 2328-2342.

[29] Salmasi, F.; Sabahi, N.; Abraham, J., Discharge coefficients for rectangular broad-crested gabion weirs: experimental study. Journal of Irrigation and Drainage Engineering 2021, 147 (3), 04021001.

[30] Seyed Mostafa Nasrollahpour Shirvani, M. G., Hamed Afrasiab, Ramazanali Jafari Talookolaei, Optimization of a Composite Sandwich Panel with Honeycomb Core Under Out-of-Plane Pressure with NMPSO Algorithm. In The 28th Annual International Conference of Iranian Society of Mechanical Engineers (ISME), 2020.

[31] Shirvani, S. M. N.; Gholami, M.; Afrasiab, H.; Talookolaei, R. A. J., Optimal design of a composite sandwich panel with a hexagonal honeycomb core for aerospace applications. Iranian Journal of Science and Technology, Transactions of Mechanical Engineering 2023, 47 (2), 557-568.

[32] Shirvani, S. M. N.; Nakhi, A.; Karimi, A.; Mobli, M., Optimizing methane direct utilization: The advanced Sr2CoMoO6-δ anode. 2023.

[33] Rensberger, J. M., Mechanical adaptation in enamel. In Tooth enamel microstructure, CRC Press: 2020; pp 237-257.

[34] Ravosa, M. J.; Klopp, E. B.; Pinchoff, J.; Stock, S. R.; Hamrick, M. W., Plasticity of mandibular biomineralization in myostatin-deficient mice. Journal of Morphology 2007, 268 (3), 275-282.

[35] Shimizu, D.; Macho, G. A.; Spears, I. R., Effect of prism orientation and loading direction on contact stresses in prismatic enamel of primates: implications for interpreting wear patterns. American Journal of Physical Anthropology: The Official Publication of the American Association of Physical Anthropologists 2005, 126 (4), 427-434.

[36] Taghavi, H.; El Shafei, A.; Nasiri, A. In Liquid Cooling System for a High Power, Medium Frequency, and Medium Voltage Isolated Power Converter, 2023 12th International Conference on Renewable Energy Research and Applications (ICRERA), IEEE: 2023; pp 405-413.

[37] Taghavi, M.; Gharehghani, A.; Nejad, F. B.; Mirsalim, M., Developing a model to predict the start of combustion in HCCI engine using ANN-GA approach. Energy Conversion and Management 2019, 195, 57-69.

[38] Taghavi, M.; Perera, L. P. In Data Driven Digital Twin Applications Towards Green Ship Operations, International Conference on Offshore Mechanics and Arctic Engineering, American Society of Mechanical Engineers: 2022; p V05AT06A028.

[39] Taghavi, M.; Perera, L. P. In Multiple Model Adaptive Estimation Coupled With Nonlinear Function Approximation and Gaussian Mixture Models for Predicting Fuel Consumption in Marine Engines, International Conference on Offshore Mechanics and Arctic Engineering, American Society of Mechanical Engineers: 2023; p V005T06A034.

[40] Lewis, G.; Nyman, J. S., The use of nanoindentation for characterizing the properties of mineralized hard tissues: State-of-the art review. Journal of Biomedical Materials Research Part B: Applied Biomaterials: An Official Journal of The Society for Biomaterials, The Japanese Society for Biomaterials, and The Australian Society for Biomaterials and the Korean Society for Biomaterials 2008, 87 (1), 286-301.

[41] Xu, H.; Smith, D.; Jahanmir, S.; Romberg, E.; Kelly, J.; Thompson, V.; Rekow, E., Indentation damage and mechanical properties of human enamel and dentin. Journal of dental research 1998, 77 (3), 472-480.

[42] Theocaris, P.; Gdoutos, E., The modified Dugdale-Barenblatt model adapted to various fracture configurations in metals. International Journal of Fracture 1974, 10, 549-564.

[43] Sun, Y.-F.; Liu, S.-B.; Meng, F.-L.; Liu, J.-Y.; Jin, Z.; Kong, L.-T.; Liu, J.-H., Metal oxide nanostructures and their gas sensing properties: a review. Sensors 2012, 12 (3), 2610-2631.